Nanoscale Deformation of a Liquid Surface

Rene Ledesma-Alonso, Dominique Legendre, and Philippe Tordjeman
Université de Toulouse, INPT, UPS, CNRS, IMFT (Institut de Mécanique des Fluides de Toulouse), Allée Camille Soula, F-31400 Toulouse, France

We study the interaction between a solid particle and a liquid interface. A semianalytical solution of the nonlinear equation that describes the interface deformation points out the existence of a bifurcation behavior for the apex deformation as a function of the distance. We show that the apex curvature obeys a simple power-law dependency on the deformation. Relationships between physical parameters disclose the threshold distance at which the particle can approach the liquid before capillarity provokes a "jump to contact." A prediction of the interface original position before deformation takes place, as well as the attraction force measured by an approaching probe, are produced. The results of our analysis agree with the force curves obtained from atomic force microscopy experiments over a liquid puddle.

In nature and manmade systems, lying on a vast domain of physics from micro- and nanofluidics, tribology, biophysics, etc., to atomic force microscopy (AFM) experiments, we often encounter situations where liquids undergo deformations due to the interaction with solid objects. Despite a significant range of object sizes, the deformation occurs at a nanoscopic scale induced by van der Waals (vdW) molecular interactions [1]. This deformation grows as the gap decreases, just before a critical distance at which the system suffers an irreversible "jump-to-contact" process and forms a capillary bridge [1,2]. Nowadays, the study of liquid properties at the nanoscale [3] based on near-field technique experiments is still a great challenge. Imaging liquids and quantifying their properties at this length scale require one to model the interaction force between liquids and nanoprobes, to determine the near-field liquid deformation, and to predict the critical distance before capillary contact. The aim of this Letter is to address all these points.

By employing an augmented Young-Laplace equation, the interface deformation due to a quasistatic approach of a particle is studied. An exact expression of the pressure field created by the vdW interaction between a sphere and a deformable surface is employed. The resulting strongly nonlinear interface equation, which includes an exact expression of the vdW volume attractive potential, is analyzed. A dimensionless treatment is made in order to generalize the problem whatever the length scale of the sphere radius. Likewise, a bifurcation diagram of the interface deformation, as well as a capillarity region corresponding to the particle-liquid wetting development, is clearly identified. Finally, by performing AFM measurements on a standard liquid polydimethylsiloxane, we validate our theoretical results and show that it is possible to predict the interface deformation, to obtain the critical distance before the capillary jump, and also to measure the Hamaker constant of a liquid with an accurate resolution up to 20 nm, which completely determines the near-field tip force.

We start by modeling the tip as a sphere of radius R, which provokes the deformation of a liquid surface originally placed at $z = 0$ (Fig. 1). The pressure difference across the interface is described by

$$2\kappa\gamma = -\Delta\rho g\eta + \Pi, \tag{1}$$

where κ is the local mean curvature, γ is the surface tension, $\Delta\rho$ is the density difference between the liquid phase and air, g is the acceleration due to gravity, and η is the interface vertical coordinate. Π is the pressure field at the interface resulting from the vdW attractive potential exerted by the whole sphere over the liquid:

$$\Pi = \frac{4HR^3}{3\pi}[(D-\eta)^2 + r^2 - R^2]^{-3}, \tag{2}$$

where H is the Hamaker constant and D is the distance from the center of the sphere to the original position of the interface. Here no assumption is made for this expression, which is obtained directly from the Hamaker theory [4]. In previous studies, the potential was approximated by

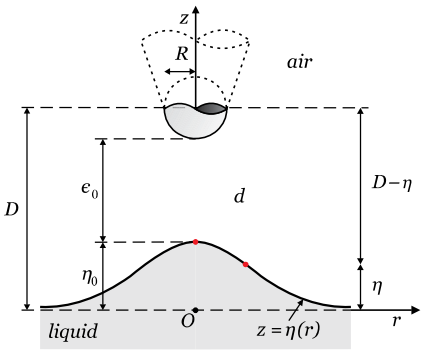

FIG. 1 (color online). Geometry of the sphere-air-liquid system.

considering a paraboloidlike microscopic tip with a local two-parallel-plate interaction [5] and a local sphere-plan interaction [6].

Taking R as the characteristic length scale of the system, we define the distance $D^* = D/R$, the horizontal $r^* = r/R$ and vertical $z^* = z/R$ coordinates, the deformation $\eta^* = \eta/R$, and the curvature $\kappa^* = \kappa R$; we also introduce the modified Hamaker number $H_a = 4H/(3\pi\gamma R^2)$ and, by using the capillary length $\lambda = \sqrt{\gamma/(\Delta\rho g)}$, the Bond number $B_0 = (R/\lambda)^2$. Typically, for ordinary AFM experiments in air, the values taken by these numbers range mostly over $H_a \in [10^{-7}, 10^{-2}]$ and $B_0 \in [10^{-11}, 10^{-8}]$. For small deformations of the interface, merging Eqs. (1) and (2) gives the dimensionless expression

$$\frac{1}{r^*}\frac{d}{dr^*}\left[\frac{r^*\frac{d\eta^*}{dr^*}}{(\frac{d\eta^*}{dr^*})^2+1}\right] = B_0\eta^* - \frac{H_a}{[(D^*-\eta^*)^2 + r^{*2} - 1]^3}. \tag{3}$$

Note that the same relation can be obtained by minimizing the total energy functional with respect to η [7].

Equation (3) is strongly nonlinear mainly due to the nature of the interaction term. A symmetry boundary condition $[\eta^*]' = 0$ is considered at $r^* = 0$. Far from the axis, at $r^*_\infty \gg 0$, where the vdW potential is negligible ($\Pi \approx 0$) and the profile is nearly flat ($[\eta^*]'_\infty \ll 1$), the boundary condition is given by the asymptotic solution of Eq. (3):

$$[\eta^*]'_\infty + \sqrt{B_0}\frac{K_1(r^*_\infty\sqrt{B_0})}{K_0(r^*_\infty\sqrt{B_0})}\eta^*_\infty = 0, \tag{4}$$

where K_0 and K_1 are zero- and first-order modified Bessel functions of the second kind.

A numerical method implemented within a MATLAB routine was used to solve Eq. (3). In Fig. 2, an example of the interface shape at equilibrium for different separating distances D^* is shown, where a "bumplike" deformation is clearly observed. The inner zone is dominated by the interaction term; hence, it is restricted to the region where the attractive influence of the sphere is significant, approximately up to $r^* = 1$. As a consequence, the external region spans from this boundary to a distance near the dimensionless capillary length $\lambda^* = 1/\sqrt{B_0}$, where the asymptotic solution perfectly describes the declining capillary behavior of the deformation. The radial extension of both regions is barely modified when increasing D^*, while, as it is reduced, the height of the profile undergoes a significant and monotonic growth. Note that the results show that $[\eta^*]' \leq 0.1$ for any r^*; hence, a linearization of the curvature in Eq. (3) can be used for simplification.

The evolution of the dimensionless height of the interface apex η^*_0 as a function of D^* is shown in Fig. 3. Depending on the initial conditions employed to solve Eq. (3), we find two different positions of the apex deformation. The lower curve is a stable branch, since it corresponds to the position which provokes the minimal

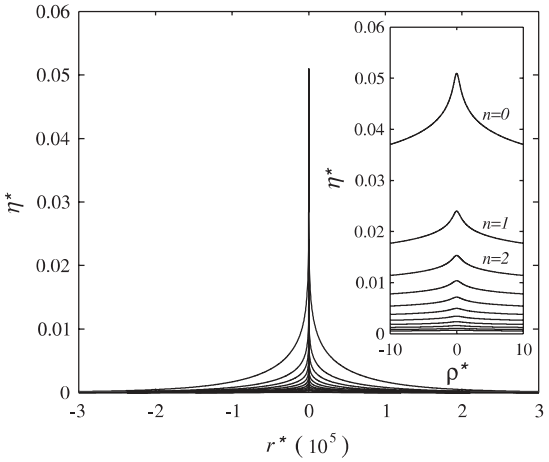

FIG. 2. Equilibrium dimensionless profiles obtained from solving Eq. (3), for $H_a = 10^{-3}$ and $B_0 = 10^{-10}$. Each curve corresponds to a profile generated with D^* equal to $(1 + n/20)D^*_{\min}$, where $n = 0, 1, 2, \ldots, 10$ and $D^*_{\min}$ is the minimum dimensionless distance at which a solution for Eq. (3) exists. Herein, $D^*_{\min} = 1.1682$ and $\eta^*_{\max} = 0.0541$.

deformation energy, whereas the upper curve indicates an unstable branch with higher energy. When D^* decreases, η^*_0 of the stable branch grows monotonically, while that for the unstable branch decreases, until a threshold distance $D^*_{\min}$, below which the slope becomes undefined. Indeed, for separation distances shorter than the bifurcation point $D^*_{\min}$, no solution for Eq. (3) is found. This behavior is confirmed by solving the dynamic evolution of the interface [8] in which the unsteadiness arises from the viscous normal stress at the interface. For $D^* < D^*_{\min}$ the instantaneous profile diverges until the sphere surface is reached, and the final equilibrium profile corresponds to a liquid bridge wetting the tip [9], while for $D^* \geq D^*_{\min}$ the stable profile given by Eq. (3) is recovered after a relaxation time $\tau = R\mu/\gamma$, μ being the liquid viscosity.

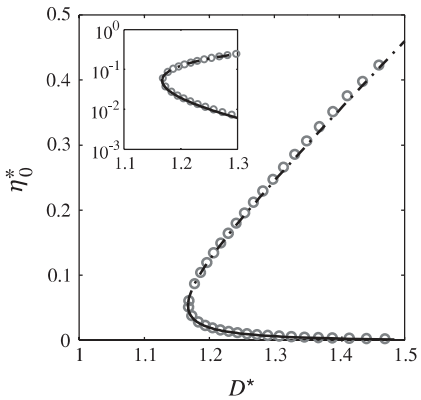

FIG. 3. Bifurcation diagram of the deformation apex for $H_a = 10^{-3}$ and $B_0 = 10^{-10}$. Solution of Eq. (3) at $r^* = 0$ (○), Eqs. (5)–(7): stable (solid line) and unstable (dash-dotted line) branches and position of the tip surface (dotted line).

For the values of B_0 considered in this study, a simple dependency of the apex curvature κ_0^* on the dimensionless height of the interface apex η_0^* is obtained empirically [8]:

$$\kappa_0^* \approx C_0 \sqrt{\frac{(\eta_0^*)^3}{H_a}}, \tag{5}$$

where $C_0 = 0.09 \pm 0.01$. Despite the complexity of the attractive potential, a very particular shape is observed at the apex. Indeed, the curvature κ_0^* is found to simply evolve as $(\eta_0^*)^{3/2}$.

From Fig. 1, we have the geometric relation

$$D^* = 1 + \eta_0^* + \epsilon_0^*, \tag{6}$$

where $\epsilon_0^* = \epsilon_0/R$ is the dimensionless gap between the sphere surface and the apex.

By considering a binomial expansion in Eq. (3) at $r^* = 0$ for the small parameter $\sqrt[3]{H_a/2\kappa_0^*}$, a second-order approximation for ϵ_0^* can be written as

$$\epsilon_0^* = \frac{1}{2}\left(\frac{H_a}{2\kappa_0^*}\right)^{1/3} - \frac{1}{8}\left(\frac{H_a}{2\kappa_0^*}\right)^{2/3}. \tag{7}$$

A good description of η_0^* as a function of D^* is obtained when combining Eqs. (5)–(7). In a bifurcation diagram (Fig. 3), the two possible stable and unstable solutions for the apex position are recovered. The minimum distance $D_{\min}^*$, at which we can approach the sphere to the interface before it "jumps," corresponds to the maximum stable deformation $\eta_{\max}^*$. This point where the branches converge also marks the distance at which the attraction potential becomes so large that the restoring surface tension and gravity forces are unable to hold it anymore, and no equilibrium profile is observed. A capillary-influenced extent, where the attractive force increases without limit and leads to the irreversible wetting process of the probe, is delimited. Finally, minimizing D^* with respect to η_0^*, we obtain $D_{\min}^* = 1 + \eta_{\max}^* + \epsilon_{\min}^*$, with

$$\eta_{\max}^* = \left[\frac{\sqrt{H_a}}{4}\left(\frac{1}{2C_0}\right)^{1/3}\right]^{2/3}, \tag{8a}$$

$$\epsilon_{\min}^* = 2\eta_{\max}^*(1 - \eta_{\max}^*). \tag{8b}$$

Therefore, $D_{\min}^*$ and $\eta_{\max}^*$ grow monotonically when increasing H_a (Fig. 4).

The sphere-liquid interaction force is equal to the addition of the deformation and the gravity forces. In turn, the deformation force is given by the derivative, with respect to η_0^*, of the deformation energy, calculated from integrating the surface deformation, as follows:

$$F_\gamma = -2\pi\gamma R^2 \frac{d}{d\eta_0^*}\left[\int_0^{\lambda^*} r^* \sqrt{1 + ([\eta^*]')^2}\, dr^* - \frac{(\lambda^*)^2}{2}\right]. \tag{9}$$

In order to validate our model, AFM experiments have been conducted. Indeed, local scanning probe techniques allow us to measure liquid interface properties with high sensitivity in a geometry close to those considered in our study [10–16]. A polydimethylsiloxane puddle with a diameter of 2 mm, a thickness of around 200 μm (considering a heavy drop analysis [17]), and a surface tension of 3.1×10^{-2} N/m was deposed on a Si/SiO_2 substrate. An Agilent Technologies 5500 scanning probe microscope was employed in contact mode to obtain the force curve over the puddle. The experiment was made by using a scanning probe Nanotools® model B1-HDC (single-crystal silicon), with a tip radius of 20 nm measured from the capillary force [2], a cantilever stiffness of 0.2 N/m deduced from thermal noise [18,19], and a resonance frequency of 15 kHz. The tip was placed near the puddle, and a force curve over the substrate was obtained. Once the calibration factor and the stiffness were calculated, the probe was retracted 225 μm and then placed above the center of the puddle. Several scanning cycles, composed of an approach-withdrawal displacement of 2 μm (motion of a piezoelectric actuator) and a subsequent automatic approach of the same size (displacement with a step motor), were then executed until the interface was reached and the tip was dipped. The force curve was carried out by taking 50 samples per nanometer and a vertical scan rate of 10 nm/s. The common resolution of an AFM is limited by the thermal noise, which takes values of around 10^{-12} N [20] at 295 K. In our experiments, this force presented a greater magnitude than thermal noise.

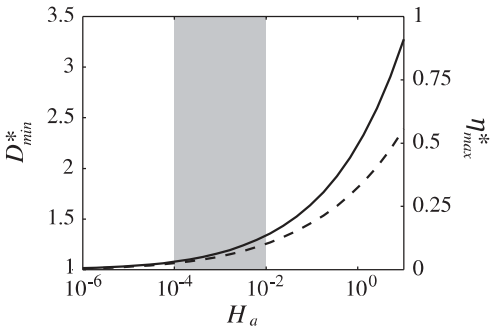

FIG. 4. Minimal dimensionless distance $D_{\min}^*$ (solid line) and apex deformation $\eta_{\max}^*$ (dashed line) as a function of H_a, corresponding to $B_0 = 1.308 \times 10^{-10}$. AFM range (shaded area).

The orders of magnitude and behaviors of theoretical and experimental force curves (Fig. 5) are in very good accordance. When the nanoscopic tip is placed far from the sample, at a distance greater than $2D_{\min}$, the deflection of the cantilever is negligible. When it approaches the interface, from $2D_{\min}$ to $D_{\min}$, the AFM measures a gradually increasing force. Within the frame of reference employed, cantilever deflections toward the interface are considered as negative values and, thus, attraction forces as well. Before reaching $D_{\min}$, the force increases abruptly, provoking a great deflection of the cantilever, which implies a magnitude of around 10^{-11} N. The gap arrives at its

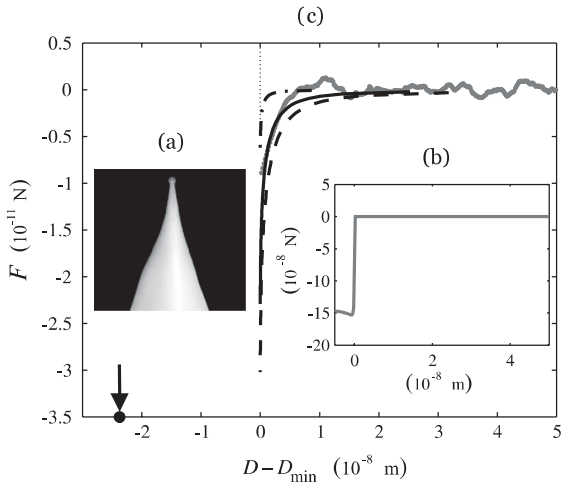

FIG. 5. (a) Tip of B1-HDC probe [23]. (b) Full view of the AFM experimental force curve for which $B_0 = 1.308 \times 10^{-10}$, corresponding to the last approach-withdrawal displacement before contact. The 0 position indicates the tip wetting. (c) Zoom of the experimental force (gray line) and the force obtained from Eq. (9) with $H = 4 \times 10^{-20}$ J (solid line), and the near values 10^{-19} (dashed line) and 10^{-21} J (dash-dotted line), corresponding to the experimental B_0. The arrow marks the position of the nondeformed liquid surface deduced from the value $D_{\min} = 24 \pm 4 \times 10^{-9}$ m calculated from Eq. (3).

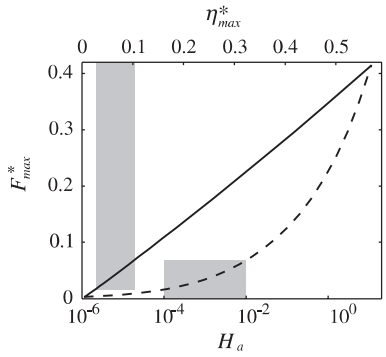

FIG. 6. Maximum dimensionless force $F^*_{\max}$ obtained from the model as a function of H_a (dashed line) and of $\eta^*_{\max}$ (solid line), corresponding to $B_0 = 1.308 \times 10^{-10}$. AFM range (shaded area).

minimum value when reaching $D_{\min}$. Hence, any separation distance smaller than $D_{\min}$ means imminent contact and the subsequent displacement of the liquid over the tip, which provokes an irreversible wetting process. The best fit is shown by the theoretical curve obtained with $H = 4 \times 10^{-20}$ J, for which $H_a = 1.4 \times 10^{-3}$, the Bond number being $B_0 = 1.308 \times 10^{-10}$. The obtained magnitude of H is very close to the value $H = 4.8 \times 10^{-20}$ J deduced from the literature [1,21,22], since the AFM measurement error is of around 20%. Consequently, a separation distance of $D_{\min} = 24 \pm 4 \times 10^{-9}$ m, at which the jump-to-contact process happens, is found. In such a way, a reference position at the nanoscopic scale is now available when scanning with an AFM probe over a liquid surface.

In Fig. 6, the maximum dimensionless force $F^*_{\max} = -F_{\max}/(R\gamma)$, as a function of H_a, shows a behavior similar to the quantities described in Fig. 4. Therefore, it exhibits a linear dependency represented by $F^*_{\max} \approx 0.7\eta^*_{\max}$, which is consistent with the fact that the surface energy follows $E \sim \gamma(R\eta^*_{\max})^2$, for small displacements of the interface.

In summary, $\eta_{\max}$, $F_{\max}$, and $D_{\min}$ increase in magnitude when increasing H. Likewise, an increase in R provokes the enlargement of $\eta_{\max}$ and $F_{\max}$; nevertheless, it causes a decrease of $D_{\min}$. For very small tips, of around $R = 1$ nm and considering $H = 10^{-20}$ J, interaction forces of the order of $F_{\max} = -3.6 \times 10^{-12}$ N are generated, which is hardly measurable with a common apparatus. In contrast, we find a significantly quantifiable $F_{\max} = -2.6 \times 10^{-11}$ N for relatively large tips of $R = 100$ nm and the same H, which strongly reduces the scanning resolution. Therefore, the resolution of AFM experiments rises when using probes with small tip radius, but their size is restricted by the minimum force measurable with an AFM. The employment of our probe-sample interaction model is suggested to obtain quantitative data from local probe measurements of liquid surfaces. Whereas a wide range of $H \in (10^{-19}, 10^{-21})$ J is commonly employed, our methodology allows us to estimate a more accurate value for a given nanoscopic tip-liquid system, when meticulous AFM measurements are performed and $F_{\max}$ is available. In addition, together with the estimation of the tip radius [2], the minimum tip-liquid distance and its corresponding deformation are obtained. Our prediction of H leads to finding the optimal distance range for scanning $D \in [D_{\min}, 2D_{\min}]$, needed to keep the interaction regime within the attractive zone before the wetting phenomenon takes control.

In this Letter, from a theoretical analysis, we have established the necessary experimental conditions to implement nanoprobe techniques when studying liquid interfaces. This work is a crucial step for imaging liquids and measuring their properties with a nanometer resolution.

[1] J. N. Israelachvili, *Intermolecular and Surface Forces* (Elsevier, New York, 2011), 3rd ed.

[2] J. Crassous, E. Charlaix, H. Gayvallet, and J. L. Loubet, Langmuir **9**, 1995 (1993).

[3] L. Bocquet and E. Charlaix, Chem. Soc. Rev. **39**, 1073 (2010).

[4] H. C. Hamaker, Physica (Utrecht) **4**, 1058 (1937).

[5] F. P.-A. Cortat and S. J. Miklavcic, Langmuir **20**, 3208 (2004).

[6] Y. Z. Wang, B. Wang, X. Xiong, and J. Zhang, Surf. Sci. **605**, 528 (2011).

[7] L. Nan, B. Yi-Long, X. Meng-Fen, and K. Fu-Jiu, Chin. Phys. Lett. **22**, 2012 (2005).

[8] See Supplemental Material at http://link.aps.org/supplemental/10.1103/PhysRevLett.108.106104 for a description of the dynamic model and the variables dependency.
[9] F. M. Orr, L. E. Scriven, and A. P. Rivas, J. Fluid Mech. **67**, 723 (1975).
[10] H. J. Butt, J. Colloid Interface Sci. **166**, 109 (1994).
[11] S. N. Magonov and D. H. Reneker, Annu. Rev. Mater. Sci. **27**, 175 (1997).
[12] A. Knoll, R. Magerle, and G. Krausch, Macromolecules **34**, 4159 (2001).
[13] F. Dutka and M. Napiorkowski, J. Phys. Condens. Matter **19**, 466104 (2007).
[14] T.-D. Li and E. Riedo, Phys. Rev. Lett. **100**, 106102 (2008).
[15] M. Delmas, M. Monthioux, and T. Ondarcuhu, Phys. Rev. Lett. **106**, 136102 (2011).
[16] J. Crassous, M. Ciccotti, and E. Charlaix, Langmuir **27**, 3468 (2011).
[17] P.-G. de Gennes, F. Brochard-Wyart, and D. Quere, *Capillarity and Wetting Phenomena: Drops, Bubbles, Pearls, Waves* (Springer, New York, 2003).
[18] B. Capella and G. Dietler, Surf. Sci. Rep. **34**, 1 (1999).
[19] J. N. Sharpe, *Handbook of Experimental Solid Mechanics* (Springer, New York, 2008).
[20] D. Smith, Rev. Sci. Instrum. **66**, 3191 (1995).
[21] K. Mougin and H. Haidara, Europhys. Lett. **61**, 660 (2003).
[22] J. Visser, Adv. Colloid Interface Sci. **3**, 331 (1972).
[23] Image provided by the manufacturer, from the Web site http://www.nanotools.com/afm-probes/ebd/general-purpose/ball-b1-b150/.